

Out-of-equilibrium photon production and electric conductivity in a holographic Bjorken expanding plasma

Sebastian Griener* and Ismail Zahed†

Center for Nuclear Theory, Department of Physics and Astronomy,
Stony Brook University, Stony Brook, New York 11794-3800, USA

(Dated: January 4, 2023)

We analytically compute the out-of-equilibrium direct photon production rate and electric conductivity, in a strongly coupled and expanding Bjorken plasma, from holography. Our results are valid at late times where the expanding plasma asymptotes Bjorken hydrodynamics. The out-of-equilibrium rates are substantially harder and larger, early on in the Bjorken expansion phase.

I. INTRODUCTION

Thermalization in heavy-ion collisions happens ultrafast (~ 1 - 2 fm/c) producing the strongly coupled quark gluon plasma (sQGP). Once produced, the sQGP undergoes transverse and longitudinal expansion which cools it, until the eventual chemical freeze-out. The time evolution in the expansion phase is described by relativistic hydrodynamics. This evolution uses an equation of state and transport coefficients (shear and bulk viscosities) which we may be extracted from flow data.

One interesting set of observables is related to the electromagnetic emissivities (photons and dileptons), which are emitted through the plasma and subsequent hadronic phase, all the way to thermal freeze-out. These direct photons and di-leptons are accessible experimentally, after the subtraction of the emissions from the late decays in the hadronic cocktail (see for example [1–4]). In contrast to the photons produced by hadronic decays in the cocktail, the direct photons – produced in all stages – give us valuable information about the time evolution of the produced matter in the collision, since they can escape the medium basically unaffected due to their substantially smaller interaction. For a snapshot of the state of the theory and currently used hydrodynamic models and parameters see [5, 6] (and references therein). Non-equilibrium photon emission rates and conductivities were studied in [7–10].

In thermal equilibrium, the electromagnetic emission is controlled by e^2 in leading order in perturbation theory, and decouples from the emitting and strongly coupled matter. Specifically, the photon

rate is given by [11, 12]

$$d\Gamma = \frac{d^3k}{(2\pi)^3} \frac{e^2}{2|\mathbf{k}|} \eta^{\mu\nu} G_{\mu\nu}^<(k) \Big|_{k^0=|\mathbf{k}|}, \quad (1)$$

where $k \equiv (k^0, \mathbf{k})$ is a null 4-vector which we put on-shell $k^0 = |\mathbf{k}|$ and

$$G_{\mu\nu}^<(k) = \int d^4x e^{i(k^0 t - \mathbf{k} \cdot \mathbf{x})} \langle J_\mu^{\text{EM}}(0) J_\nu^{\text{EM}}(x) \rangle \quad (2)$$

is the Wightman function for the electric current de-correlation. In thermal equilibrium, the Wightman function $G_{\mu\nu}^<$ is related to the spectral density $\chi_{\mu\nu}$ using the Bose-Einstein distribution $n_b(k^0) = 1/(e^{\beta k^0} - 1)$

$$G_{\mu\nu}^<(k) = n_b(k^0) \chi_{\mu\nu}(k) \quad (3)$$

$$= -\frac{2}{e^{\beta k^0} - 1} \text{Im} G_{\mu\nu}^R(k), \quad (4)$$

Here $G_{\mu\nu}^R(k)$ is the retarded electric current correlator in Fourier space.

Modelling the non-equilibrium dynamics of strongly coupled field theories from first principles is a notoriously difficult problem. In this context, holography proved to be a valuable framework to study the real-time evolution, and transport properties of certain strongly coupled field theories (see [13] for a discussion in the context of heavy-ion collisions). Within holography, the dynamics of the strongly coupled field theory is captured by general relativity in asymptotically Anti-de Sitter space. In this language, thermalization is described by the formation of a black hole [14], whose horizon is moving away from a boundary observer [15]. We will rely on the picture of the falling black hole, to extract the out-of-equilibrium photon production during the cooling process.

Bjorken [16] suggested a highly successful model for the central rapidity region of heavy-ion reactions,

* sebastian.griener@stonybrook.edu

† ismail.zahed@stonybrook.edu

based on boost invariant hydrodynamics. The holographic dual gravity model which is based on the idea of the falling black hole in [15], was constructed in [17, 18]. The main idea is to map the falling black hole onto a frame where the horizon is static and we can define (a time dependent) temperature [18]. The static frame provides a well defined framework for linear response theory. For example [19, 20] used this idea to compute the diffusion of heavy quarks in these expanding backgrounds.

Within holography, the equilibrium: photon and dilepton production in $\mathcal{N} = 4$ super Yang-Mills plasma was calculated in [12]. In holographic models for QCD (in the Veneziano limit) the photon production was derived in [21, 22]. The authors in [23] extended the holographic discussion to anisotropic plasmas with magnetic fields. The authors in [24] computed the gradient corrections to the photon emission rate at strong coupling. Out-of-equilibrium, the prompt photon and dilepton production was discussed in [25, 26], using the holographic model of a falling shell. However, in the context of the falling shell the background metric is not explicitly time dependent, and connects smoothly to the equilibrium case which allows the authors to rely on Fourier transformations. In this work, we will compute the out-of-equilibrium photon production in a time dependent background corresponding to a strongly coupled, Bjorken expanding plasma. Correlation functions of the Bjorken flow in the context of the holographic Schwinger-Keldysh approach were discussed in [27].

The organization of the paper is as follows: In section II we briefly review the holographic set up for a falling black hole in bulk, dual to boost invariant Bjorken hydrodynamics on the boundary. We analyze the evolution of a $U(1)$ vector gauge field, and derive the on-shell boundary action from which the pertinent retarded propagator on the boundary can be extracted. In section III, we use the holographic result to derive the photon emission rate in a Bjorken expanding and strongly coupled plasma. In section IV we derived a closed form result for the $U(1)$ electric conductivity in out-of-equilibrium. Our conclusions are in V.

II. HOLOGRAPHIC SETUP

In the following, we study a strongly coupled $SU(N_c)$ $\mathcal{N} = 4$ super-Yang Mills theory at finite

temperature and zero density. In order to study the photon production rate and conductivity, we couple a $U(1)$ gauge field in terms of a Maxwell term to gravity where we assume the electromagnetic coupling to be small. To be more precise, the $U(1)$ group is a subgroup of the global $SU(4)$ \mathcal{R} -symmetry.

The metric describing the asymptotic expanding fluid geometry is given by [17, 18].

$$ds^2 = \frac{R^2}{z^2} \left[-\frac{(1-v^4)^2}{1+v^4} d\tau^2 + (1+v^4)(\tau^2 d\eta^2 + dx_\perp^2) + dz^2 \right], \quad (5)$$

where $x_\perp = \{x_1, x_2\}$ are the transverse directions, $z \in \{0, 1\}$ is the radial coordinate of AdS_5 , τ is the proper time, η the rapidity related to the longitudinal directions by $x^0 = \tau \cosh \eta$ and $x_3 = \tau \sinh \eta$, where x^0 is the time coordinate. Moreover, we set the radius of AdS and the horizon to unity. The scaling variable v is given by

$$v = \frac{z}{(\tau/\tau_0)^{1/3}} \epsilon_0^{1/4}, \quad \epsilon_0 \equiv \frac{1}{4} (\pi T_0)^4, \quad (6)$$

where ϵ_0 is the initial energy density and T_0 the initial temperature. Note that the horizon is located at $v = 1$ or $z \sim \tau^{1/3}$. Following [19], we can transform the metric into a more canonical form, which resembles a static black hole. Introducing $u(z, \tau) \equiv 2v^2/(1+v^4)$ yields

$$ds^2 = \frac{\pi^2 T_0^2 R^2}{u (\tau/\tau_0)^{2/3}} [-f(u) d\tau^2 + \tau^2 d\eta^2 + dx_\perp^2] \quad (7) \\ + \frac{R^2}{4f(u)} \frac{du^2}{u^2} + \frac{R^2}{9\tau^2} d\tau^2 - \frac{R^2}{3} \frac{\tau^{-1}}{u\sqrt{f(u)}} d\tau du,$$

with $f = 1 - u^2$. At late times where the perfect fluid geometry is valid (i.e. $\tau \rightarrow \infty$ and $v, u = \text{const}$), the last two terms are suppressed, and can be ignored. Finally, rescaling the time coordinate by $t/t_0 = 3/2 (\tau/\tau_0)^{2/3}$ yields

$$ds^2 = \frac{\pi^2 T_0^2 R^2}{u} \left(-f(u) \frac{\tau_0^2}{t_0^2} dt^2 + \frac{4}{9} t^2 \frac{\tau_0^2}{t_0^2} d\eta^2 + \frac{3}{2} \frac{t_0}{t} dx_\perp^2 \right) \\ + \frac{R^2}{4f(u)} \frac{du^2}{u^2}. \quad (8)$$

Using this background, we now consider the vector perturbations $\delta a = (\delta a_t, 0, \delta a_{x_\perp}, \delta a_\eta)$ of a $U(1)$ gauge field in radial gauge ($x_\perp = \{x_1, x_2\}$) which is captured by the bulk action

$$S_{\text{matter}} = -\frac{1}{4e^2} \int d^5x \sqrt{-g} F_{\mu\nu} F^{\mu\nu}, \quad (9)$$

where $F = da$. For now we will set the electromagnetic coupling $e = 1$ and recover it when we compute the transport quantities. At late times, there is no

dependence on the transverse directions, and therefore we will only consider the dependence on the longitudinal direction. The equation of motion for the transverse fluctuations reads $a_{x_\perp} \equiv a_{x_\perp}(t, \eta, u)$

$$4\pi^2 \tilde{T}_0^2 u f(u) (f'(u) \partial_u a_{x_\perp} + f(u) \partial_u^2 a_{x_\perp}) - \partial_t^2 a_{x_\perp} - \frac{\partial_t a_{x_\perp}}{t} + \frac{9f(u) \partial_\eta^2 a_{x_\perp}}{4t^2} = 0, \quad (10)$$

where we defined $\tilde{T}_0 \equiv T_0 \tau_0 / t_0$. The dependence on the longitudinal direction η is subleading at late times, and we can neglect it. Since the equation of motion explicitly depends on time we cannot use a simple Fourier transform, but have to perform a separation of variables by making the ansatz

$$a_{x_\perp} = c g_1(t) g_2(u) \quad (11)$$

where we find that we can separate the time dependence with

$$g_1(t) = c_1 {}_0\tilde{F}_1 \left(; 1; -\frac{1}{32} (3t^2 \lambda) \right) + c_2 Y_0 \left(\frac{1}{2} \sqrt{\frac{3}{2}} t \sqrt{\lambda} \right).$$

Here λ, c_1, c_2 are independent of t, u , ${}_0\tilde{F}_1$ is the regularized confluent hypergeometric function, and Y_0 refers to Bessel functions. Choosing the constants c_1 and c_2 accordingly, we eventually arrive at the expression

$$g_1(t) = H_0^{(2)}(\omega t), \quad (12)$$

which satisfies the in-going boundary condition at the horizon. We now define a Fourier-like transform using

$$a_{x_\perp}(t, u) = \int_{-\infty}^{\infty} \frac{d\omega}{2\pi} \sqrt{\frac{i\pi\omega}{2}} H_0^{(2)}(\omega t) \psi_\omega(u) \tilde{a}_{x_\perp}(\omega), \quad (13)$$

where $\psi_\omega(0) = 1$. We will drop the subscript of $\psi \equiv \psi_\omega$ in the following. With $\lambda = \omega$ and $g_2 = \psi$, we find for the spatial part

$$\frac{4u\pi^2}{\tilde{T}_0^{-2}} (u^2 - 1) ((u^2 - 1)\psi''(u) + 2u\psi'(u)) + \omega^2 \psi(u) = 0 \quad (14)$$

which we will solve in the following.

A. Analytical solution

The solution to the equation of motion (14) should behave as an in-going wave at the horizon. Since the horizon is a regular singular point, we can expand the near horizon solution in a power series

$$\psi(u) \sim (1 - u)^\alpha (1 + \dots), \quad (15)$$

where $\alpha = \pm \frac{i\omega}{4\pi\tilde{T}_0}$. We can recast eq. (14) formally as a Heun's differential equation which is solved by the hypergeometric functions

$$\begin{aligned} \psi_\omega(u) = & -ic_2 \left(-\frac{1}{2} \right)^{\frac{i\omega}{2\pi\tilde{T}_0}} (u-1)^{\frac{i\omega}{4\pi\tilde{T}_0}} (u+1)^{\frac{\omega}{4\pi\tilde{T}_0}} u^{-\frac{(\frac{1}{4} + \frac{i}{4})\omega}{\pi\tilde{T}_0}} {}_2F_1 \left(\frac{(\frac{1}{4} + \frac{i}{4})\omega}{\pi\tilde{T}_0}, \frac{(\frac{1}{4} + \frac{i}{4})\omega}{\pi\tilde{T}_0} + 1; \frac{i\omega}{2\pi\tilde{T}_0} + 1; \frac{u-1}{2u} \right) \\ & - ic_1 (u-1)^{-\frac{i\omega}{4\pi\tilde{T}_0}} (u+1)^{\frac{\omega}{4\pi\tilde{T}_0}} u^{-\frac{(\frac{1}{4} - \frac{i}{4})\omega}{\pi\tilde{T}_0}} {}_2F_1 \left(\frac{(\frac{1}{4} - \frac{i}{4})\omega}{\pi\tilde{T}_0}, \frac{(\frac{1}{4} - \frac{i}{4})\omega}{\pi\tilde{T}_0} + 1; 1 - \frac{i\omega}{2\pi\tilde{T}_0}; \frac{u-1}{2u} \right). \end{aligned} \quad (16)$$

The solution satisfying the in-going boundary con-

dition at the horizon is the one proportional to c_1 ,

which implies $c_2 = 0$. Demanding that $\psi_\omega(0) = 1$ (since we are interested in the two point function)

determines the second integration constant c_1 , and we find

$$\psi_\omega(u) = 2^{-\frac{(\frac{1}{4}-\frac{i}{4})\omega}{\pi\tilde{T}_0}} e^{-\frac{\omega}{4\tilde{T}_0}} \Gamma\left(1 - \frac{(\frac{1}{4} + \frac{i}{4})\omega}{\pi\tilde{T}_0}\right) \Gamma\left(\frac{(\frac{1}{4} - \frac{i}{4})\omega}{\pi\tilde{T}_0} + 1\right) (u-1)^{-\frac{i\omega}{4\pi\tilde{T}_0}} u^{-\frac{(\frac{1}{4}-\frac{i}{4})\omega}{\pi\tilde{T}_0}} (u+1)^{\frac{\omega}{4\pi\tilde{T}_0}} \quad (17)$$

$$\times {}_2\tilde{F}_1\left(\frac{(\frac{1}{4} - \frac{i}{4})\omega}{\pi\tilde{T}_0}, \frac{(\frac{1}{4} - \frac{i}{4})\omega}{\pi\tilde{T}_0} + 1; 1 - \frac{i\omega}{2\pi\tilde{T}_0}; \frac{u-1}{2u}\right), \quad (18)$$

where ${}_2\tilde{F}_1(a, b; c, d)$ is the regularized hypergeometric function ${}_2\tilde{F}_1(a, b; c, d)/\Gamma(c)$.

In our ansatz, the on-shell action gives rise to the boundary term

$$S_{\text{on-shell}} = \frac{\pi^4 R^5 \tau_0^2 T_0^4}{4 t_0 u^3} \int d^3x dt A_n F^{un} \Big|_{u=0}^{u=1} \quad (19)$$

$$= \int \frac{d\omega}{2\pi} \tilde{a}_{x_\perp}(-\omega) \left[-\frac{2\pi^2}{3} R \tilde{T}_0^2 f(u) \psi_{-\omega} \psi'_\omega \right]_{u=0}^{u=1} \tilde{a}_{x_\perp}(\omega), \quad (20)$$

where we assumed

$$-\frac{1}{4} \int_{-\infty}^{\infty} dt t H_0^{(2)}(\omega t) H_0^{(2)}(-\omega' t) \simeq \frac{1}{\omega} \delta(\omega - \omega'), \quad (21)$$

which is valid for small ω . To first order in u the

$$G^R(\omega) = \frac{4\pi^2}{3} R \tilde{T}_0^2 [f(u) \psi_{-\omega}(u) \psi'_\omega(u)]_{u=0} = -\frac{R}{3} \omega \left(H\left(\frac{\frac{1}{4}-\frac{i}{4}}{\pi\tilde{T}_0}\omega\right) + \psi^{(0)}\left(-\frac{(\frac{1}{4} + \frac{i}{4})\omega}{\pi\tilde{T}_0}\right) + \gamma + \log(2) - 2\pi\tilde{T}_0 \right), \quad (22)$$

where γ is the Euler number, $H(n)$ is the n th harmonic number H_n , and $\psi^{(n)}(z)$ is the n th derivative of the digamma function. In general, the symmetrized Wightman function $G(\omega)$ in momen-

asymptotic expansion at the conformal boundary reads $\psi \sim \psi_{(\mathbf{s})} + u \left(\psi_{(\mathbf{v})} - \frac{\psi_{(\mathbf{s})} \omega^2 \log(u)}{4\pi^2 \tilde{T}_0^2} \right)$. To extract the expectation value, we have to subtract the logarithmic contribution by adding the appropriate counter term. The pre-factor of the logarithmic contribution enters the expectation value of the current as $\langle J_{x_\perp} \rangle \sim \left(\psi_{(\mathbf{v})} - \omega^2 \psi_{(\mathbf{s})} / (8\pi^2 \tilde{T}_0^2) \right)$. This contact term does not affect the photon production rate, or the real part of the conductivity, since they are related to the imaginary part of the retarded Green's function. It contributes, however, to the imaginary part of the conductivity. From eq. (20), we can then read off the renormalized retarded Green's function $G_R(\omega)$ as

tum space is related to the imaginary part of retarded Green's function via $G(\omega) = -\coth(\omega/(2\tilde{T}_0)) \text{Im} G_R(\omega)$ [28]. On the one hand, we find for the electric conductivity at small frequencies $\omega \ll \tilde{T}_0$

$$\sigma = \frac{1}{i\omega} G^R(\omega) = \frac{2\pi R}{3} \tilde{T}_0 + \frac{1}{3} i R \log(2) \omega + \frac{R \pi \omega^2}{36 \tilde{T}_0} + \frac{R \pi \omega^4}{4320 \tilde{T}_0^3} + \mathcal{O}(\omega^5) \quad (23)$$

On the other hand, for large frequencies $\omega \gg \tilde{T}_0$, we find

$$\sigma = \frac{1}{i\omega} G^R(\omega) = -\frac{16i\pi^4 R \tilde{T}_0^4}{45\omega^3} + \frac{2}{3} i R \omega \left(-\log(\pi \tilde{T}_0) + \log(\omega) + \gamma - i\pi/2 - \log(2) \right) + \mathcal{O}\left(\frac{1}{\omega^6}\right). \quad (24)$$

These results are obtained in the frame where the

black hole is static, and are in general in agreement

with the conductivity of the Schwarzschild AdS₅ black hole in [29] (see appendix A). Note that the normalization of the metric differs compared to the Schwarzschild case.

B. Connecting to the boosted frame

So far, we worked with the frequency ω with respect to the time t , in the frame where the black hole is static. In order to compute the photon production rate, we have to convert our result to frequencies with respect to the proper time in the Bjorken frame. We may define an inverse Fourier transform according to

$$G(t_1, t_2) = -\frac{1}{4} \int_{-\infty}^{\infty} d\omega \omega H_0^{(2)}(\omega t_1) H_0^{(2)}(-\omega t_2) G(\omega). \quad (25)$$

If we introduce the relative and CM coordinates

$$s = t_1 - t_2, \quad \mathcal{T} = \frac{t_1 + t_2}{2}, \quad (26)$$

we find that for $t_1, t_2 \gg 1$

$$G = -\frac{1}{2\pi \sqrt{t_1 t_2}} \int_0^{\infty} d\omega e^{-i(t_1 - t_2)\omega} G(\omega) \quad (27)$$

$$= -\frac{1}{\mathcal{T}} \frac{1}{\sqrt{1 - \frac{s^2}{4\mathcal{T}^2}}} \int \frac{d\omega}{2\pi} e^{-i\omega s} G(\omega). \quad (28)$$

The relative time is related to the proper time by

$$s = 3/2 s_0 (\tau/\tau_0)^{2/3} = \tilde{\tau}_0 \tau^{2/3}$$

with $\tilde{\tau}_0 = 3/2 s_0 \tau_0^{-2/3}$. With this in mind, we find

$$\begin{aligned} G &= -\frac{1}{\mathcal{T}} \frac{1}{\sqrt{1 - \frac{s^2}{4\mathcal{T}^2}}} \int \frac{d\omega}{2\pi} e^{-i\frac{\tilde{\tau}_0}{\tau^{1/3}}\omega} G(\omega) \quad (29) \\ &= -\frac{1}{\mathcal{T}} \frac{1}{\sqrt{1 - \frac{s^2}{4\mathcal{T}^2}}} \int \frac{dq^0}{2\pi} \frac{2\tilde{T}_0}{3T(\tau)} e^{-iq^0\tau} G\left(\frac{2\tilde{T}_0 q^0}{3T}\right), \quad (30) \end{aligned}$$

where we introduced

$$q^0 = \omega \tilde{\tau}_0 \tau^{-1/3}, \quad d\omega = \tau^{1/3}/\tilde{\tau}_0 dq^0$$

and used $T = T_0/(\tau/\tau_0)^{1/3}$ [19].

The 4-momentum of the photon is given by

$$q^\mu = (m_T \cosh(y - \eta), m_T, m_T \sinh(y - \eta)), \quad (31)$$

where y is the photon rapidity in the Bjorken frame with rapidity η . The number of photons per unit volume, unit rapidity and mass in the Bjorken frame, is given by

$$q^0 \frac{d\Gamma}{[d\tau \tau d\eta dx_\perp] [d^3q]} = \frac{d\Gamma}{dV_{\text{Bj}} dy dm_T^2/2} \quad (32)$$

It is related to the frame where the black hole horizon is fixed by

$$q^0 \frac{d\Gamma}{[d\tau \tau d\eta dx_\perp] [d^3q]} = \omega \frac{d\Gamma}{dV_{\text{bh}} [d^3k]}. \quad (33)$$

III. OUT-OF-EQUILIBRIUM DIRECT PHOTON PRODUCTION RATE

In the following, we elaborate how our solution for the retarded Green's function of the transverse gauge field fluctuations is connected to the photon production rate (2). We can decompose the spectral function of the \mathcal{R} current according to [12]

$$G_{\mu\nu}^R(k) = P_{\mu\nu}^T(k) \Pi^T(k^0, k) + P_{\mu\nu}^L(k) \Pi^L(k^0, k), \quad (34)$$

with the transverse and longitudinal projector

$$P_{00}^T = 0 = P_{0i}^T, \quad P_{ij}^T(k) = \delta_{ij} - k_i k_j / \mathbf{k}^2$$

$$P_{\mu\nu}^L(k) = P_{\mu\nu}(k) - P_{\mu\nu}^T(k)$$

Taking the trace yields

$$\chi_\mu^\mu(k^0, k) = -4\text{Im}\Pi^T(k^0, k) - 2\text{Im}\Pi^L(k^0, k). \quad (35)$$

In general, the transverse and the longitudinal part contribute to the spectral function. However, we are interested in on-shell photons. For light-like momenta, the longitudinal part vanishes, and the photon-production rate is totally determined by the transverse part. Therefore, the rate of photon production per unit rapidity and mass, is given by integrating over the fluid spatial evolution

$$\begin{aligned} \frac{d\Gamma}{dy dm_T^2/2} &= \int d\tau (\tau d\eta) dx_\perp \frac{d\Gamma}{dV_{Bj} dy dm_T^2/2} \\ &= \frac{2\pi R_T^2}{\mathcal{T}} \int_{\tau_i}^{\tau_f} d\tau \frac{1}{\sqrt{1 - \frac{s^2}{4\mathcal{T}^2}}} \tau \int_{\eta_{\min}}^{\eta_{\max}} d\eta \frac{2\tilde{T}_0 n_b(\mathfrak{w}(\tau, \eta))}{3T(\tau)} \text{Im} G_{a_{x_\perp} a_{x_\perp}}^R(\mathfrak{w}(\tau, \eta)), \end{aligned} \quad (36)$$

$$\mathfrak{w}(\tau, \eta) \equiv \frac{2\tilde{T}_0 m_T}{3T} \cosh(y - \eta), \quad (37)$$

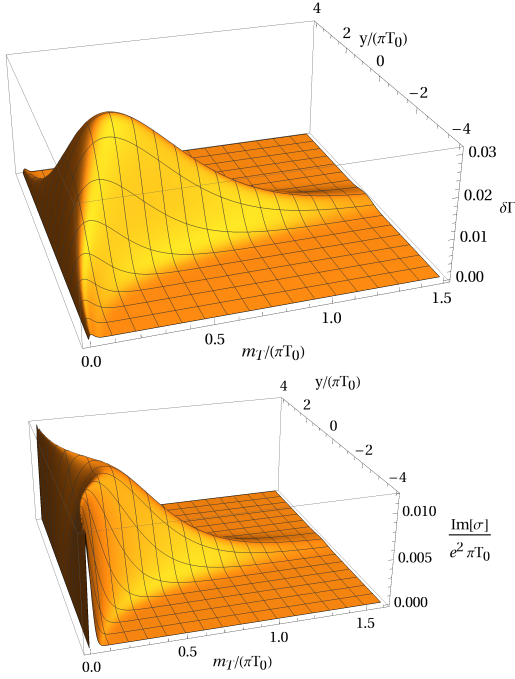


FIG. 1:

$\tau = 5/(\pi\tilde{T}_0)$, $\tilde{T}_0 = 1/\pi$, $\eta = 0$, $\tau_0 \pi\tilde{T}_0 = 1$, $R = 1$.

Upper panel: Produced photons

$\delta\Gamma \equiv \frac{m_T}{(e\pi\tilde{T}_0)^3} \frac{d\Gamma}{dV dy dm_T^2/2}$ as a function of the photon momentum and rapidity. For small m_T and η the

data are proportional to the real part of the out-of-equilibrium electrical conductivity. *Lower*

panel: The imaginary part of the out-of-equilibrium electrical conductivity.

where n_b is the Bose-Einstein distribution discussed in eq. (4). In figure 1, we display the integrand

$$\delta\Gamma \equiv \frac{m_T}{(e\pi\tilde{T}_0)^3} \frac{d\Gamma}{dV dy dm_T^2/2}$$

For $\mathfrak{w} \ll \tilde{T}_0$, we find

$$\begin{aligned} \frac{2\tilde{T}_0 n_b}{3T} \text{Im} G^R &= \frac{8\pi R \tilde{T}_0^2}{9} \\ &+ \frac{\mathfrak{w} \left(-12T\tilde{T}_0^2 + \mathfrak{w}(T^2 + 2\tilde{T}_0^2) \right)}{27T^2/(\pi R)} + \dots, \end{aligned} \quad (38)$$

which agrees with the scaling behavior of the equilibrium calculation [12]. Note that s_0 related to the initial relative time.

In figure 2, we illustrate the dependence of the photon production on the proper time (and thus on the temperature for a given energy density). Starting from the green curve which corresponds to the smallest proper time $\tau = 2$, the maximum shifts to lower momenta m_T and decreases in magnitude. The red curve corresponds to $\tau = 10$. This is in strong contrast to the result of [25] which considered a non-expanding plasma.

IV. OUT-OF-EQUILIBRIUM CONDUCTIVITY

The retarded current-current correlator also contains the information about the electrical conductivity σ of the expanding plasma, which is encoded in the zero frequency limit. More specifically, we have by [12]

$$\sigma = - \lim_{k^0 \rightarrow 0} \frac{e^2}{4i\tilde{T}_0} \frac{2}{e^{k^0/T} - 1} G_{x_\perp x_\perp}^R(k) \Big|_{|\mathbf{k}|=k^0}. \quad (39)$$

Thus, the real part of the conductivity is given by (38). In summary, the out-of-equilibrium conductivity is given by

$$\begin{aligned} \frac{\sigma}{e^2} &= \frac{\pi R T}{3} + \frac{iR\mathfrak{w}(T \log(2) + i\pi\tilde{T}_0)}{6\tilde{T}_0} \\ &+ \frac{R\mathfrak{w}^2 \left(\pi \left(T^2 + 2\tilde{T}_0^2 \right) - iT\tilde{T}_0 \log(64) \right)}{72T\tilde{T}_0^2}. \end{aligned} \quad (40)$$

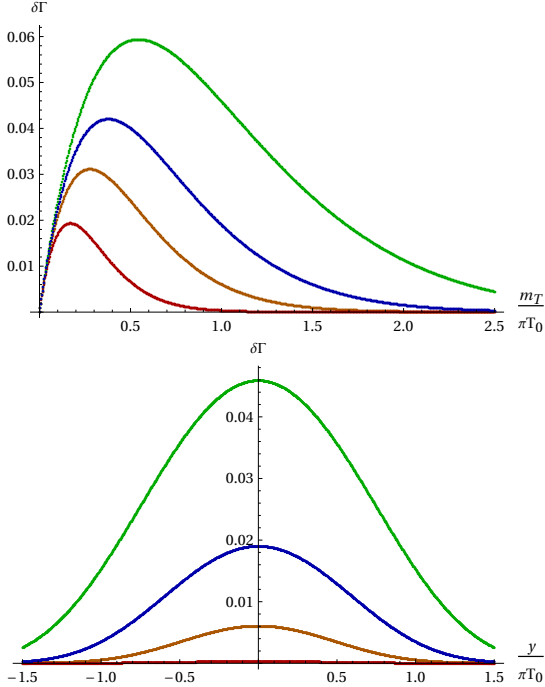


FIG. 2: $\tau = \{2, 3.25, 5, 10\}/(\pi\tilde{T}_0)$ (green, blue, brown, red), $\tilde{T}_0 = 1/\pi, \eta = 0, \tau_0 \pi\tilde{T}_0 = 1, R = 1$. *Upper panel*: Produced photons $\delta\Gamma \equiv \frac{m_T}{(e\pi\tilde{T}_0)^3} \frac{d\Gamma}{dV dy dm_T^2/2}$ as a function of the photon momentum for different proper times indicated by different colors. We set $y = 0$. *Lower panel*: We set $m_T = \pi\tilde{T}_0$ and study the dependence on the pseudo-rapidity y for different proper times.

The conductivity has dimensions of temperature. In figure 3, we illustrate the dependence of the real and imaginary part of the conductivity on the proper time (and thus on the temperature for a given energy density). Starting from the green curve which corresponds to the smallest proper time $\tau = 2$, the value of the real part at $m_T = 0$ decreases for larger proper times. Furthermore, the real part drops more rapidly as a function of the photon momentum m_T for increasing proper time. The maximum in the imaginary part of the conductivity, moves towards lower frequencies and decreases in magnitude for increasing proper time from green to red. We also note that the peak is slightly more pronounced for $\tau = 10$.

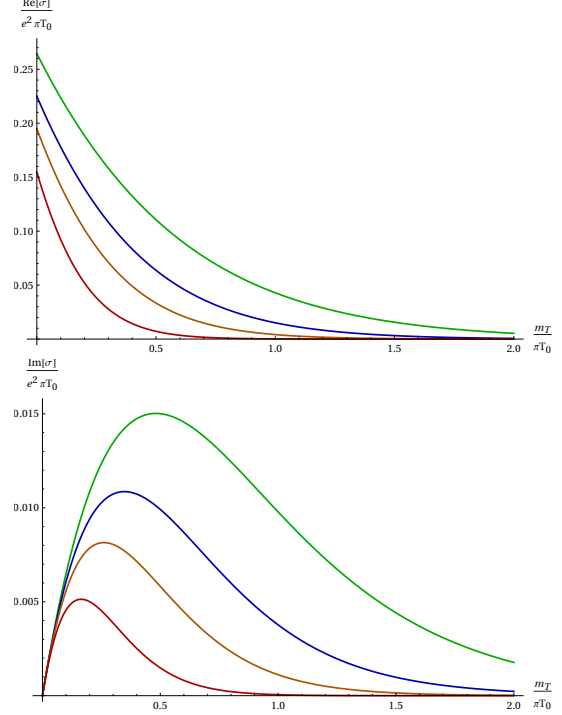


FIG. 3: $\tau = \{2, 3.25, 5, 10\}/(\pi\tilde{T}_0)$ (green, blue, brown, red), $T_0 = 1/\pi, \eta = 0, \tau_0 \pi\tilde{T}_0 = 1, R = 1$. Real and imaginary part of the conductivity for different proper times and $y = 0$.

V. CONCLUSIONS

In this work, we derived the out-of-equilibrium direct photon production rate and electrical conductivity, for an expanding Bjorken plasma. At late times, our results agree with the literature, however, by deriving the quantities in the time dependent background our results incorporate the history of the Bjorken expansion, and are dependent on the proper time and pseudo-rapidity. Since our metric is explicitly time dependent it is not possible to rely on Fourier transforms. However, in the Bjorken limit, we were able to re-cast the metric in the form of a static black hole, and factor out the time dependence with a Fourier-like transform based on Hankel functions. This trick, which is valid for moderate frequencies, allows us to compute the out-of-equilibrium transport quantities analytically.

We illustrated the dependence of the direct photon production rate on proper time, pseudo-rapidity, and photon momentum. At fixed pseudo-rapidity the peak in the production rate moves to lower momenta, for increasing proper time and is progres-

sively suppressed. We observed a similar behavior for the imaginary part of the electrical conductivity. The real part of the conductivity for zero momenta decreases towards larger proper times as we would expect for an expanding plasma. Furthermore, it tends to zero at larger momenta.

Our results provide analytical insight into the out-of-equilibrium transport of an expanding Bjorken plasma. It would be very interesting to extend our results to finite density along the lines of [30, 31], and eventually strong background magnetic fields. Another interesting direction is to study metric fluctuations in order to compute transport quantities like the shear viscosity. Moreover, it would be interesting to consider non-Abelian symmetries to compute pion yields in heavy ion collisions with holographic techniques. Furthermore, it would be interesting to compute correction to our setup in the fluid/gravity correspondence context. We leave these tasks for future work.

Finally, the out-of-equilibrium conductivity was studied in the AdS/CMT context in [32, 33] and it would be interesting to relate the results.

Acknowledgements: S.G. is supported by the U.S. Department of Energy, Office of Science grant No. DE-FG88ER41450. I.Z. is supported by the Office of Science, U.S. Department of Energy under Contract No. DE-FG-88ER40388.

Appendix A: Conductivity in Schwarzschild AdS₅

The metric of the AdS₅ Schwarzschild black hole reads

$$ds^2 = \frac{R^2}{u^2} \left(-f(u) dt^2 + d\mathbf{x}^2 + \frac{du^2}{f(u)} \right). \quad (\text{A1})$$

To compute the conductivity, we consider gauge field fluctuations about this background. The analytical solution to the gauge field equations in Fourier space at zero wave-vector and finite frequency ω , is given by [29] and reads

$$a_x = \left(\left(\frac{1}{u} \right)^2 - 1 \right)^{-i\omega/4} \left(\left(\frac{1}{u} \right)^2 + 1 \right)^{-\omega/4} {}_2F_1 \left(\frac{1}{4}(-1+i)\omega, 1 - \frac{1}{4}(1+i)\omega; 1 - \frac{i\omega}{2}; \frac{1}{2} \left(1 - \frac{1}{u^2} \right) \right). \quad (\text{A2})$$

The renormalized retarded Green's function may be read off from

$$G^R(\omega) = - \lim_{u \rightarrow 0} \frac{R f(u) a_x a'_x}{u}, \quad (\text{A3})$$

after subtracting the logarithmic divergence. As we

noted earlier, the coefficient of the logarithm contributes a contact term to the imaginary part of the conductivity. Thus, the conductivity which is defined as $\sigma = G^R/(i\omega)$ (where we have set $T_c = \pi T$ in [29]), is given by

$$\sigma = -R\pi T + i\omega R \left[\frac{1}{2} \psi \left(\frac{(1-i)\omega}{4\pi T} \right) + \frac{1}{2} \psi \left(-\frac{(1-i)\omega}{4\pi T} \right) + \frac{1}{2} \log(2) + \gamma \right], \quad (\text{A4})$$

where $\psi(u) = \Gamma'(u)/\Gamma(u)$ is the di-gamma function. The conductivity may be expanded in the limit of small and large frequencies compared to the temper-

ature. The small frequency limit $\omega \ll T$ reads [29]

$$\sigma = T \left(\pi + i \log(2) \frac{\omega}{2T} + \mathcal{O}(\omega^2) \right), \quad (\text{A5})$$

while the large frequency limit $\omega \gg T$ is given by [29]

$$\sigma = R\omega \left(\frac{\pi}{2} + i \left(\log \frac{\omega}{2\pi T} + \gamma \right) + \mathcal{O}(\omega^{-4}) \right). \quad (\text{A6})$$

-
- [1] A. Adare *et al.* (PHENIX), *Phys. Rev. C* **91**, 064904 (2015), [arXiv:1405.3940 \[nucl-ex\]](#).
- [2] S. Afanasiev *et al.* (PHENIX), *Phys. Rev. Lett.* **109**, 152302 (2012), [arXiv:1205.5759 \[nucl-ex\]](#).
- [3] A. Adare *et al.* (PHENIX), *Phys. Rev. Lett.* **104**, 132301 (2010), [arXiv:0804.4168 \[nucl-ex\]](#).
- [4] J. Adam *et al.* (ALICE), *Phys. Lett. B* **754**, 235 (2016), [arXiv:1509.07324 \[nucl-ex\]](#).
- [5] J.-F. Paquet, C. Shen, G. S. Denicol, M. Luzum, B. Schenke, S. Jeon, and C. Gale, *Phys. Rev. C* **93**, 044906 (2016), [arXiv:1509.06738 \[hep-ph\]](#).
- [6] C. Gale, *PoS High-pT2017*, 023 (2019), [arXiv:1802.00128 \[hep-ph\]](#).
- [7] S. Hauksson, S. Jeon, and C. Gale, *Phys. Rev. C* **97**, 014901 (2018).
- [8] M. Greif, F. Senzel, H. Kremer, K. Zhou, C. Greiner, and Z. Xu, *Phys. Rev. C* **95**, 054903 (2017), [arXiv:1612.05811 \[hep-ph\]](#).
- [9] A. Schäfer, J. M. Torres-Rincon, C. Gale, and H. Elfner, *Nucl. Phys. A* **1005**, 121772 (2021), [arXiv:2001.03378 \[nucl-th\]](#).
- [10] Y. Yin, *Phys. Rev. C* **90**, 044903 (2014), [arXiv:1312.4434 \[nucl-th\]](#).
- [11] J. V. Steele, H. Yamagishi, and I. Zahed, *Phys. Rev. D* **56**, 5605 (1997), [arXiv:hep-ph/9704414](#).
- [12] S. Caron-Huot, P. Kovtun, G. D. Moore, A. Starinets, and L. G. Yaffe, *JHEP* **12**, 015 (2006), [arXiv:hep-th/0607237](#).
- [13] E. V. Shuryak, *Nucl. Phys. A* **750**, 64 (2005), [arXiv:hep-ph/0405066](#).
- [14] H. Nastase, (2005), [arXiv:hep-th/0501068](#).
- [15] E. Shuryak, S.-J. Sin, and I. Zahed, *J. Korean Phys. Soc.* **50**, 384 (2007), [arXiv:hep-th/0511199](#).
- [16] J. D. Bjorken, *Phys. Rev. D* **27**, 140 (1983).
- [17] R. A. Janik and R. B. Peschanski, *Phys. Rev. D* **73**, 045013 (2006), [arXiv:hep-th/0512162](#).
- [18] R. A. Janik and R. B. Peschanski, *Phys. Rev. D* **74**, 046007 (2006), [arXiv:hep-th/0606149](#).
- [19] K.-Y. Kim, S.-J. Sin, and I. Zahed, *JHEP* **04**, 047 (2008), [arXiv:0707.0601 \[hep-th\]](#).
- [20] A. Stoffers and I. Zahed, *Phys. Rev. C* **86**, 054905 (2012), [arXiv:1110.2943 \[hep-th\]](#).
- [21] I. Iatrakis, E. Kiritsis, C. Shen, and D.-L. Yang, *JHEP* **04**, 035 (2017), [arXiv:1609.07208 \[hep-ph\]](#).
- [22] I. Iatrakis, E. Kiritsis, C. Shen, and D.-L. Yang, *Nucl. Part. Phys. Proc.* **289-290**, 177 (2017), [arXiv:1612.05114 \[nucl-th\]](#).
- [23] I. Y. Aref'eva, A. Ermakov, and P. Slepov, *Eur. Phys. J. C* **82**, 85 (2022), [arXiv:2104.14582 \[hep-th\]](#).
- [24] K. A. Mamo and H.-U. Yee, *Phys. Rev. D* **91**, 086011 (2015), [arXiv:1409.7674 \[nucl-th\]](#).
- [25] R. Baier, S. A. Stricker, O. Taanila, and A. Vuorinen, *Phys. Rev. D* **86**, 081901 (2012), [arXiv:1207.1116 \[hep-ph\]](#).
- [26] R. Baier, S. A. Stricker, O. Taanila, and A. Vuorinen, *JHEP* **07**, 094 (2012), [arXiv:1205.2998 \[hep-ph\]](#).
- [27] A. Banerjee, T. Mitra, and A. Mukhopadhyay, (2022), [arXiv:2207.00013 \[hep-th\]](#).
- [28] D. T. Son and A. O. Starinets, *JHEP* **09**, 042 (2002), [arXiv:hep-th/0205051](#).
- [29] G. T. Horowitz and M. M. Roberts, *Phys. Rev. D* **78**, 126008 (2008), [arXiv:0810.1077 \[hep-th\]](#).
- [30] T. Kalaydzhyan and I. Kirsch, *JHEP* **02**, 053 (2011), [arXiv:1012.1966 \[hep-th\]](#).
- [31] T. Kalaydzhyan and I. Kirsch, *Phys. Rev. Lett.* **106**, 211601 (2011), [arXiv:1102.4334 \[hep-th\]](#).
- [32] A. Bagrov, B. Craps, F. Galli, V. Keränen, E. Keski-Vakkuri, and J. Zaanen, *Phys. Rev. D* **97**, 086005 (2018), [arXiv:1708.08279 \[hep-th\]](#).
- [33] A. Bagrov, B. Craps, F. Galli, V. Keränen, E. Keski-Vakkuri, and J. Zaanen, *JHEP* **07**, 065 (2018), [arXiv:1804.04735 \[hep-th\]](#).